Environ Earth Sci (2012) 65:1029–1036
DOI 10.1007/s12665-011-1358-4

SPECIAL ISSUE

Evolution of shear zones using numerical analysis at the May 12th Wenchuan Earthquake Site, China

X. B. Lu · P. Cui · X. Q. Chen · K. H. Hu · Y. Y. Zhu

Received: 15 March 2010 / Accepted: 10 September 2011 / Published online: 24 September 2011
© Springer-Verlag 2011

Abstract Landslides and collapses occurred during the May 12th earthquake in Wenchuan County. Most of these landslides and collapses were caused by shear bands. Shear band triggers instability on mountain slopes, resulting in debris flow, landslides, or collapse. According to experimental results, there was only one shear band forming in the soil layer prior to the initiation of debris flow under shear load, although several fine shear bands appeared. The development of shear bands in saturated soils is numerically investigated in this paper using the in situ soil from the Weijia Gully, Beichuan County. The evolution of shear banding from several finite amplitude disturbances (FADs) in pore pressure has been studied. The numerical analysis revealed that the FADs evolved into a fully developed shear band. It is shown that the shear banding process consists of two stages: inhomogeneous shearing and true shear banding.

Keywords Simple shear · Saturated soils · Shear bands · Instability

List of symbols

*	Within the band
τ	Shear stress
γ	Shear strain
p	Pore pressure
ρ_w	Density of water
ρ	Density of grains
L	Length of the specimen
g	Earth's gravity acceleration
μ	Viscosity of water
k	Darcy permeability
C_1	Material parameter
E_r	Compressible modulus of grains
t_h, t_d	Characteristic times
δ	Half width of shear band
a, b, d	Dimensionless parameters
a_1, l, m, n	Constant coefficients
p_δ	Pore pressure at boundary

X. B. Lu (✉)
Institute of Mechanics, Chinese Academy of Sciences, Beijing 100080, China
e-mail: xblu@imech.ac.cn

P. Cui · X. Q. Chen · K. H. Hu · Y. Y. Zhu
Institute of Mountain Hazards and Environment, Chinese Academy of Sciences, Chengdu 610041, Sichuan, China

Introduction

Sand deposits on a slope can create a landslide because of the development of shear band (Cui 1992; Cui et al. 2008; Vardoulakis 2002). During the May 12th earthquake in Wenchuan, the amount of landslides was developed step by step from shear band to the sliding surface of a landslide, even if there are several bands first (Fig. 1; Cui et al. 2008; Cheng et al. 2009). Therefore, the initiation of shear band has a direct relationship to the occurrence of landslides. Shear bands occur quite frequently in saturated soils under dynamic or static loading conditions and have attracted considerable attention for many years. Among the wealth of literature on this subject, works by Rice (1975), Vardoulakis (1985), Ottosen and Runesson (1991), Runesson et al. (1991, 1996), and Rice and Cleary (1976) are mentioned. The necessary conditions for discontinuous bifurcations have been established by their works. Ottosen and Runesson (1991), Runesson et al. (1996), Tejchman and Wu (1996),

Fig. 1 A landslide in Beichuan

and Bauer et al. (2004) presented the analytical and numerical results that included general elastic–plastic models. Shear band formation in saturated soils may be described as follows: the strain rate increases, resulting in the build-up of high pore pressure and the decrease of the effective stresses. Under these conditions, the deformation of the saturated soils may develop to shear banding. However, how does the shear band evolve in saturated soils? Why is there only a single shear band occurring at the later stage in a specimen even if there are several bands occurring at the first stage? All these questions are of great importance and many have researched these questions in recent years (Runesson et al. 1998; Lu et al. 2000, 2004; Lu 2001; Vardoulakis 1986; Lu and Cui 2003; Loret and Provest 1991).

This paper aims to investigate the evolution of shear bands in saturated soils numerically at Beichuan County after the 5.12 earthquake in 2008. The focus of the discussion is on the evolution of the inhomogeneous shear to ultimate band, which creates the sliding surface of a landslide or a collapse. The whole process is divided into two stages: the coalescence stage of several fine shear bands and the localization stage that forms a single shear band.

Numerical model and simulation

Numerical model

Although the above model sheds light on the mechanism of shear band in saturated soils, it is oversimplified and does not accurately reflect real-world scenarios. To investigate the process in detail, numerical simulations and experiments were performed (Bai 1982; Xing et al. 1991; Lade et al. 1988; Lade 1994; Vardoulakis and Graf 1985; Peric et al. 1992; Pietruszczak 1995). Careful examinations of the same specimen revealed several fine shear bands that were distributed over the deformed region (Fig. 2). However, only one fully developed shear band appeared prior to collapse.

The finite difference method was implemented to study the instability and the subsequent processes of shear banding in this paper. As shown in Fig. 3, a block with a length of L was deformed by a constant driving velocity under undrained boundary conditions. The specimen was initially homogeneous and strain-free.

The inertial and elastic effects can be neglected during the process of shear banding. For deformation that is homogeneous on the scale of specimen, the shear stress τ is only a function of time, thus the equations governing the specimen deformation are as follows (Oda and Kazama 1998):

$$\frac{\partial \tau}{\partial x} = 0 \tag{1}$$

Plastic deformation acts as a source of pore pressure, and the generation rate of pore pressure is proportional to the plastic work rate $\tau\dot{\gamma}$. Thus, the one-dimensional pore pressure diffusion equation becomes:

$$C_1 E_r \tau \dot{\gamma} = \frac{\partial p}{\partial t} - \frac{E_r}{K}\frac{\partial^2 p}{\partial y^2} \tag{2}$$

in which p is the pore pressure, E_r is the unloading modulus, $K = \rho_w g/k$, is ρ_w the density of water, k is the Darcy permeability, g is the Earth's gravity acceleration, C_1 is a material parameter, and ρ is the density of saturated soils mixture.

Here the following type of constitutive equation (Lu and Cui 2003; lshibli and Sture 2000; Aifantis 1987) was developed:

$$\tau = a\gamma^m \dot{\gamma}^n p^\lambda. \tag{3}$$

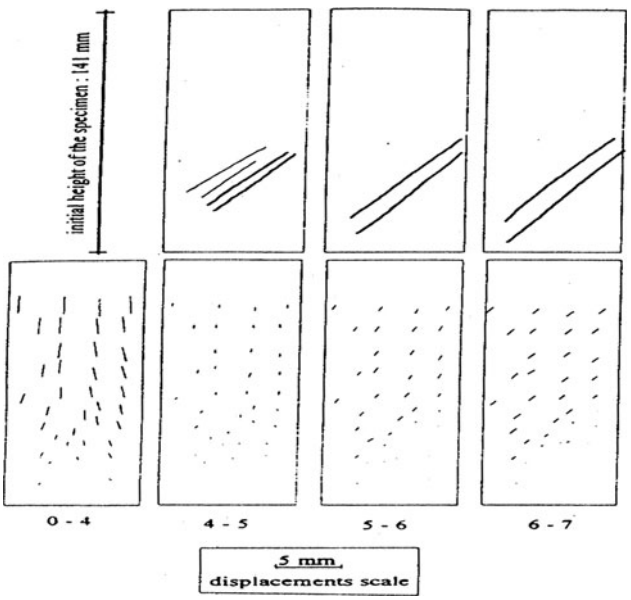

Fig. 2 X-ray images of shear bands (Peric et al. 1992)

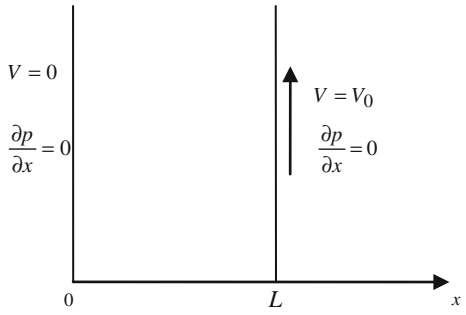

Fig. 3 Schematic diagram of deformed region

Assuming an undrained condition at the specimen's ends because of rapid deformation and a clamped end, the boundary conditions of pore pressure were:

$$\left.\frac{\partial p}{\partial x}\right|_0 = \left.\frac{\partial p}{\partial x}\right|_L = 0. \tag{4}$$

The specimen was clamped at $x = 0$ and constrained to move at a velocity V_0 at $x = L$,

$$\int_0^L \dot{\gamma} dx = V_0. \tag{5}$$

The specimen was strain-free initially at $t = 0$, e.g.:

$$\gamma(x, 0) = 0. \tag{6}$$

The initial strain rate at $t = 0$ was:

$$\dot{\gamma}(x, 0) = \dot{\gamma}_0 = V_0/L. \tag{7}$$

The initial pore pressure in the specimen was the same everywhere:

$$p(x, 0) = p_0. \tag{8}$$

Now, the non-dimensional form of the above governing equations and boundary conditions and initial conditions were obtained by using the following non-dimensional variables:

$$\bar{x} = x/\Delta,\ \bar{t} = \dot{\gamma}_0 t,\ \tau = \bar{\tau}\tau_b,\ \bar{\tau} = \tau/\tau_0,\ \bar{p} = p/p_0,$$

$$Q = \frac{1}{C_1 K \Delta^2 \dot{\gamma}_0},\ R = \frac{1}{E_r C_1},\ B = \frac{A\gamma_0^m \dot{\gamma}_0^n \theta_0^v}{\tau_0},\ a = L/\Delta$$

in which Δ is the characteristic width of a shear band, τ_0 is the characteristic shear strength, and p_0 is the characteristic pore pressure.

Equations 1–8 may be normalized by substituting the above non-dimensional variables as follows:

$$\bar{\tau} = \bar{\tau}(t) \tag{9}$$

$$\bar{\tau}\dot{\bar{\gamma}} = R\frac{\partial \bar{p}}{\partial \bar{t}} - Q\frac{\partial^2 \bar{p}}{\partial \bar{y}^2} \tag{10}$$

$$\bar{\tau} = B\bar{\gamma}^m \dot{\bar{\gamma}}^n \bar{p}^v \tag{11}$$

$$\left.\frac{\partial \bar{p}}{\partial \bar{x}}\right|_0 = \left.\frac{\partial \bar{p}}{\partial \bar{x}}\right|_a = 0 \tag{12}$$

$$\frac{1}{a}\int_0^a \dot{\gamma}(\bar{x}, \bar{t}) dx = 1 \tag{13}$$

$$\gamma(x, 0) = 0 \tag{14}$$

$$\dot{\gamma}(x, 0) = 1 \tag{15}$$

$$\bar{p}(x, 0) = 1 \tag{16}$$

The over-bar used to indicate a dimensionless variable is omitted in the following sections for simplicity.

Numerical methodology

In phase I ($0 < t < t_s$), it is supposed that the specimen deformed uniformly as the pore pressure rose homogeneously. Then, γ, $\dot{\gamma}$, p, τ was found analytically.

At $t = t_s$, a number of finite amplitude disturbance (FADs) were introduced into the distribution of pore pressure. Each disturbance was a Gauss distribution in x axial, distinguished by its position, half width and disturbing energy.

In phase II ($t_s < t < t_e$), numerical calculations were carried out to simulate the process in which FADs evolved into shear bands. The details of the numerical methodology were given below.

1. For $0 < t < t_s$, the specimen deformed homogeneously and the pore pressure also increased homogeneously, i.e.

$$\frac{\partial p}{\partial x} = \frac{\partial \gamma}{\partial x} = \frac{\partial \dot{\gamma}}{\partial x}. \tag{17}$$

The governing equations at this stage were:

$$\frac{dp}{dt} = c\tau\dot{\gamma} \tag{18}$$

$$\tau = a\gamma^m \dot{\gamma}^n p^v \tag{19}$$

$$\gamma = \dot{\gamma}_0 t \tag{20}$$

$$\dot{\gamma} = \dot{\gamma}_0 = 1 \tag{21}$$

$$p|_{t=0} = p_0 \tag{22}$$

Integrating these equations with respect to time, the following was obtained:

$$p = \left[\frac{1-v}{1+n} cat^{n+1} + p_0^{1-v}\right]^{1/(1-v)}. \tag{23}$$

2. Time $t = t_s$, disturbances of finite amplitude in pore pressure were introduced into the homogeneous

background (Fig. 4). After the disturbance, the pore pressure distribution can be theoretically calculated using:

$$p\left(x,t_s^+\right)=p_b+\sum_{i=1}^{N}a_i f_i(x) \tag{24}$$

in which N denotes the number of disturbances, $f_i(x)$ denotes the distribution function and a_i denotes the magnitude of the ith FAD. In this paper, $f_i(x)$ is a Gauss function,

$$f_i(x)=\exp\left[-\frac{(x-x_i)^2}{\Delta x_i^2}\right] \tag{25}$$

in which Δx_i is the characteristic half width and x_i is the location of the ith FAD. It is supposed that $2\Delta x_i << a$ (i.e. disturbances have a short wavelength). Therefore, it may be obtained that:

$$\int_0^a f_i(x)dx=\int_{-\infty}^{+\infty}\exp\left[-\frac{(x-x_i)^2}{\Delta x_i^2}\right]dx=\sqrt{\pi}\Delta x_i. \tag{26}$$

If the time interval between t_s^- and t_s^+ is so small that:

(a) the strain state of the block in Fig. 3 remains unchanged,
(b) the total energy of the block does not change,
(c) elastic and inertial effects can be neglected,
(d) the constant velocity and undrained boundary conditions remain true, then

$$\gamma\left(x,\ t_s^-\right)=\gamma\left(x,\ t_s^+\right) \tag{27}$$

$$\int_0^a p\left(x,\ t_s^-\right)dx=\int_0^a p\left(x,\ t_s^+\right)dx \tag{28}$$

$$\int_0^a \dot{\gamma}\left(x,\ t_s^-\right)dx=\int_0^a \dot{\gamma}\left(x,\ t_s^+\right)dx \tag{29}$$

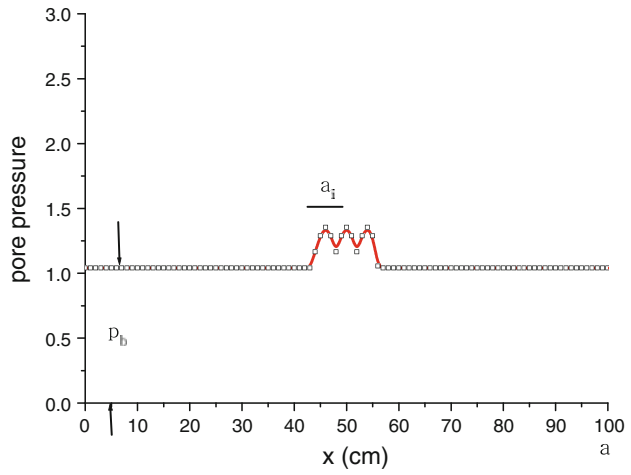

Fig. 4 Schematic diagram of disturbed pore pressure distribution

$$\left.\frac{\partial p}{\partial t}\right|_0=\left.\frac{\partial p}{\partial t}\right|_a=0 \tag{30}$$

$$\tau=A\dot{\gamma}^m\gamma^n p^v \tag{31}$$

Thus, each FAD in pore pressure is distinguished by its position x_i, its half width Δx_i and the percentage concentration energy E_i. Here E_i is defined as:

$$E_i=\frac{\text{energy concentrated in the ith FAD}}{\text{total energy}}=\frac{a_i\int_0^a f_i(x)dx}{\int_0^a p(x,\ t_s)dx} \tag{32}$$

By solving Eqs. 27–31, the following results are obtained:

$$a_i=\left[E_i\int_0^a p\left(x,\ t_s^-\right)dx\right]\Big/\left(\sqrt{\pi}\Delta x_i\right) \tag{33}$$

$$p_b=\frac{1}{a}\left(1-\sum_{i=1}^{N}E_i\right)\int_0^a p\left(x,\ t_s^-\right)dx \tag{34}$$

$$p\left(x,\ t_s^+\right)=p_b+\sum_{i=1}^{N}a_i f_i(x). \tag{35}$$

From Eq. 31 and Eq. 35, γ, $\dot{\gamma}$ and τ at t_s^+ can be found analytically as follows:

$$\gamma\left(x,\ t_s^+\right)=\gamma\left(x,\ t_s^-\right) \tag{36}$$

$$\dot{\gamma}=\left[\frac{\tau}{A\gamma^n p^v}\right]^{1/m}\Bigg|_{t=t_s^+} \tag{37}$$

Now, it is very clear that, for a given N, E_i, x_i and Δx_i, the disturbed $\theta\left(x,\ t_s^+\right), \dot{\gamma}\left(x,\ t_s^+\right), \gamma\left(x,\ t_s^+\right)$ and $\tau\left(t_s^+\right)$ from Eqs. 35 to 37 may be found.

3. For time $t_s<t<t_e$, a numerical calculation was carried out, based on Eqs. 9–16, to simulate the process, in which FADs evolve into a shear band. Numerical integration and Green's function for an undrained boundary were used. Eq. 10 was rewritten as:

$$\frac{\partial p}{\partial t}=R\tau\dot{\gamma}+P\frac{\partial^2 p}{\partial x^2}. \tag{38}$$

Here it is subjected to the same boundary conditions and constitutive relations as before.

Numerical simulation

To investigate the shear banding process in detail, a number of numerical simulations were carried out.

The parameters using in Eqs. 10–16 had to be determined before a numerical simulation could take place.

Thus the in situ soils in Weijia Gully in Beichuan County were used to analyze the areas' physical and mechanical properties. The grain sizes of the soils were widely distributed as shown in Fig. 5. The dry density was 15.79 kg/m^3. A static and dynamic triaxial apparatus was used to determine the parameters of constitutive relation. There was no peak in the curves of axial strain and deviatoric stress (Fig. 6). The internal friction angle and the cohesion can be obtained by Mohr circles as 12° and 150 kPa, respectively. Under dynamic loading, the soil can develop to liquefaction (Fig. 7). From the curves of pore pressure versus time and remnant stress versus time, the changes of the strength and pore pressure can be obtained. Therefore, the relation between the pore pressure and the strength can be analyzed. Then, the parameters a, R, m, n, v, P can be obtained.

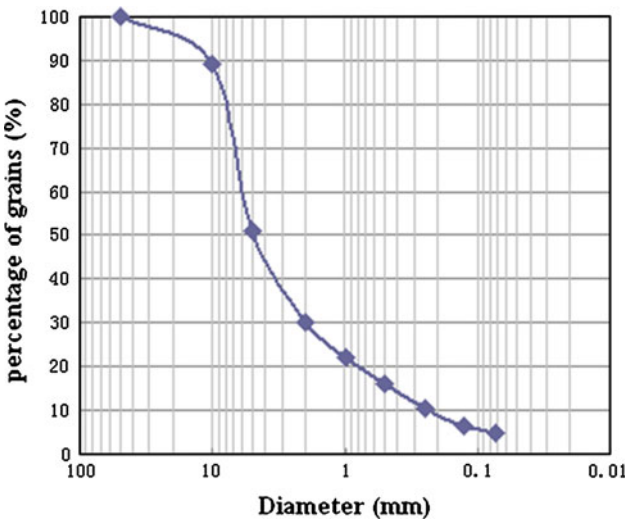

Fig. 5 Grain series curves for Wenchuan soils

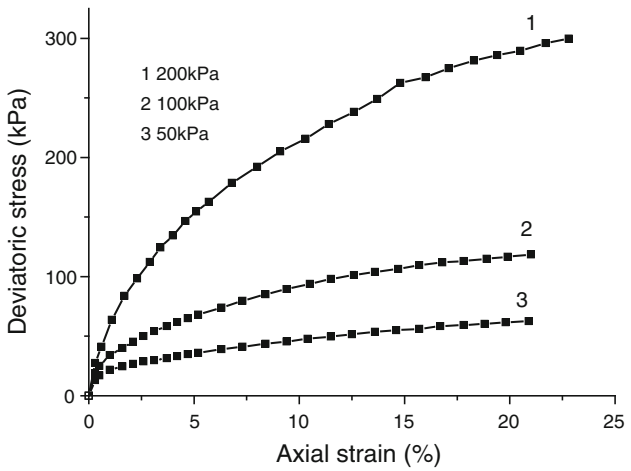

Fig. 6 Axial strain versus deviatoric stress

The material parameters used in computation were adopted as follows according to the test results:

$$R = 2.5 \times 10^{-3},\ Q = 2.5 \times 10^{-6},\ A = 1.1 \times 10^{-5},$$
$$m = 0.5,\ n = 0.5,\ v = -2,\ p_0 = 1.0.$$

First of all, calculation to show the effect of different mesh sizes on the features of the shear banding process was carried out. Figure 8 shows the relationship of dimensionless stress and local shear strain at the center of shear band versus nominal shear strain rate (two disturbances were applied). It is shown that when the stress began to decrease (initiation of shear band), the strain rate increased rapidly.

To simulate a number of fine shear bands appearing near the experimentally observed stress peak, up to three FADs with a total energy ranging from 0.1 to 3% were adopted in computation. All cases showed similar late-stage behavior, namely a single shear band appearing in the deformed region. A typical evolution is shown in Fig. 9. Three FADs gradually merged into a contracted localized area at about $\gamma = \gamma_l = 0.2$ (γ_l was the strain at which the stress begins to drop), where a drastic decrease of disturbed stress occurred. Afterwards, as the shear strain rate and the pore pressure of the shear band increased rapidly, the band shrank. Finally, the ultimate shear band was formed, showing a quite stable band width, despite the fact that the pore pressure diffused

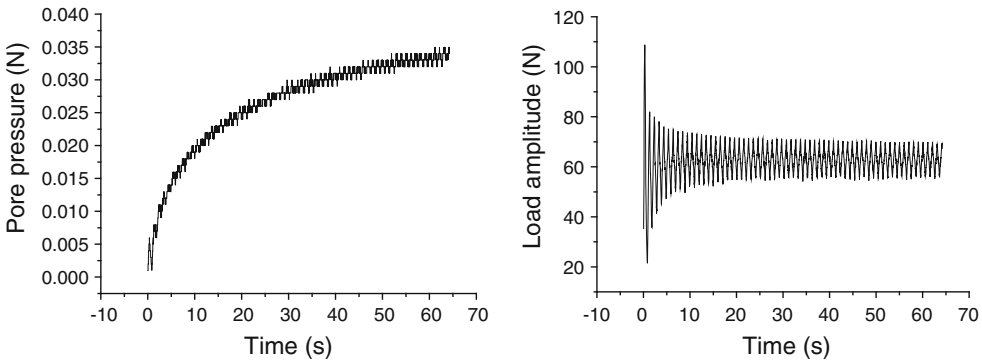

Fig. 7 The development of pore pressure with time under dynamic loading. **a** Changes of pore pressure; **b** changes of remnant stress

(a) Changes of pore pressure

(b) Changes of remnant stress

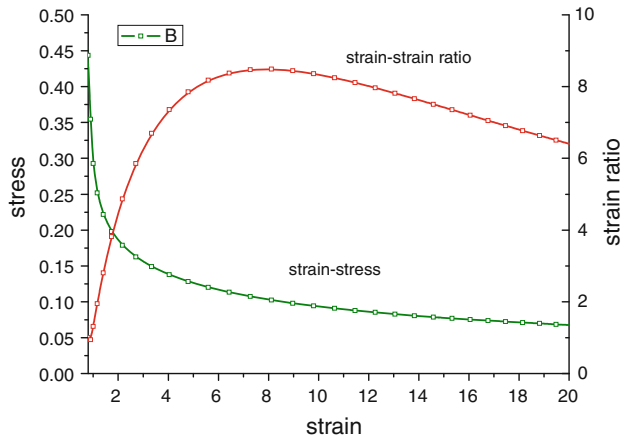

Fig. 8 Stress versus strain and strain rate

continuously. The width of the final shear band was found to be independent of the FADs chosen.

The mesh sizes chosen in calculation have little effect on the features of the shear banding process, including the width of the final developed shear band.

For analysis of the two stages from the application of FADs to the final shear band, a detailed simulation of the process of shear banding revealed that there were two distinct stages (Fig. 8) separated by γ_l. During the first stage ($\gamma < \gamma_l$), the stress evolved close to that of the uniform solution (Fig. 8). The shear during the second stage ($\gamma > \gamma_l$) caused severe localization. The shear band shrank to its final form (Fig. 10), the stress dropped drastically and the strain rate at the center of shear band increased sharply at first (Fig. 8). Therefore, the first stage can be thought of as the coalescence stage and the second stage as the localization stage.

Figure 11 shows the effect of disturbance energy on the value of γ_l. The value of γ_l decreased as the disturbance energy E increased. Disturbances with low energy (0.5%) decreased faster than those with high energy (3.0%). These results suggest the importance of investigating the effects of short wavelength disturbances with low disturbance energy on shear banding after reaching the maximum of the stress–strain curve.

Furthermore, the effects of the distribution of FADs on the position and the time to reach γ_t were studied. The site

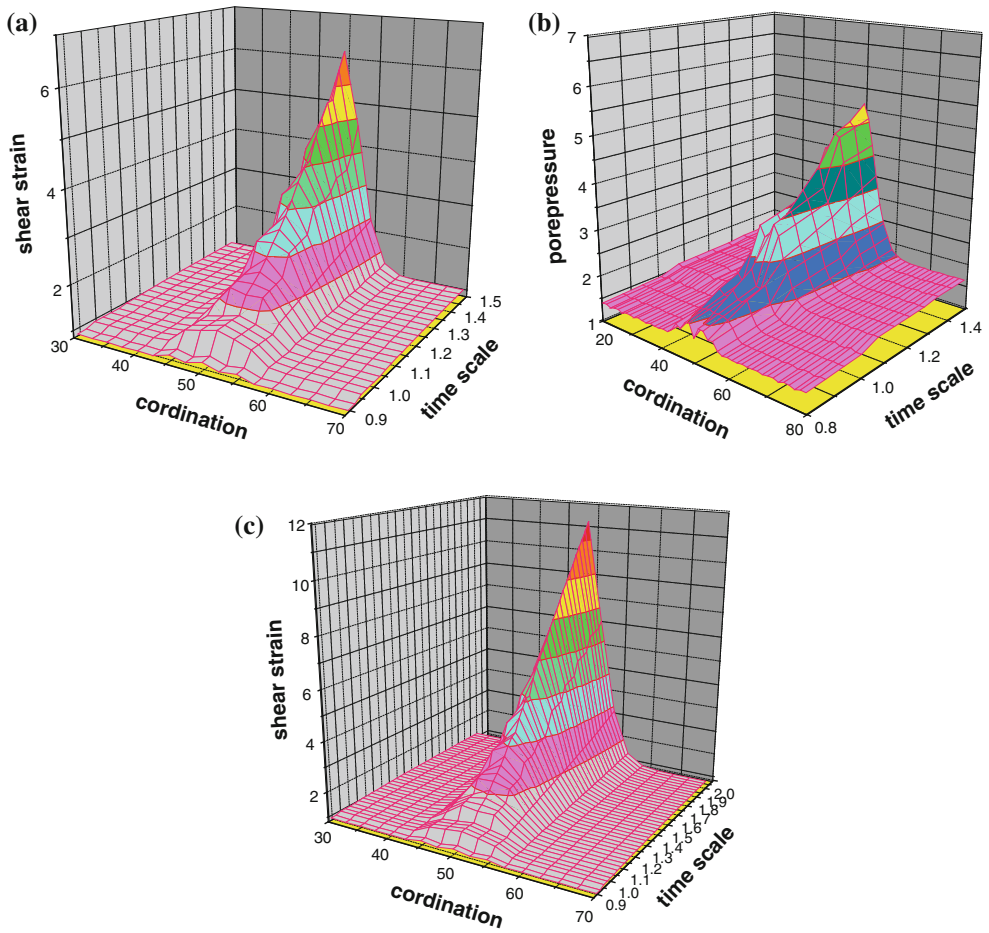

Fig. 9 Evolution of one shear band from three FADs. **a** Strain-rate evolution, **b** pore pressure evolution, **c** strain evolution

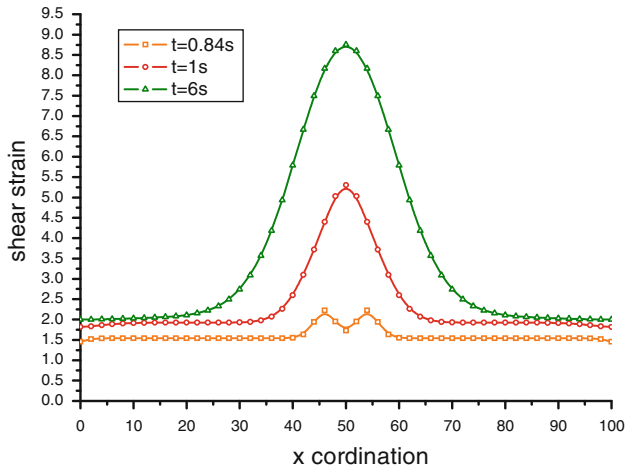

Fig. 10 Localization process at different nominal strain

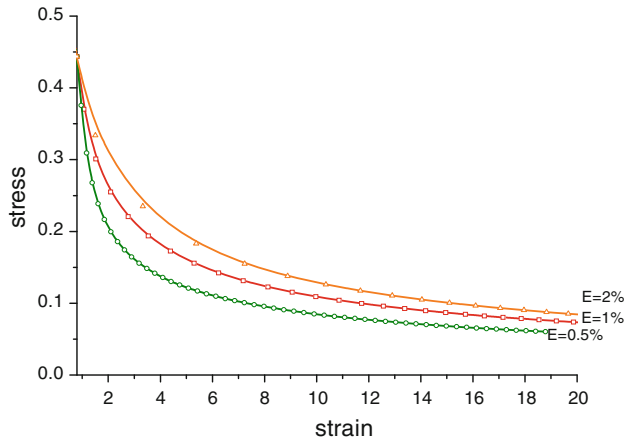

Fig. 11 The effect of disturbance energy E on γ_l

of localization, i.e. the position of the final developed single shear band, was dependent on the distribution of FADs, but did not correspond to any individual FAD. A typical result is shown in Fig. 12. There, three FADs with total energy of 1% were applied initially at $\gamma_s = 0.2$. Through an energy complicated evolution process, the final developed shear band appeared at $\gamma = 0.5$, which had a different position from the location of any individual FAD.

Conclusions

The process of shear banding was studied using a numerical simulation. Numerical integration was used to investigate the evolution of finite amplitude disturbances (FADs). In the range of $0 < \gamma < \gamma_l$, even when some disturbances were imposed, no shear localization occurred in the numerical simulations. When disturbances with very low energy were applied, no shear localizations appeared

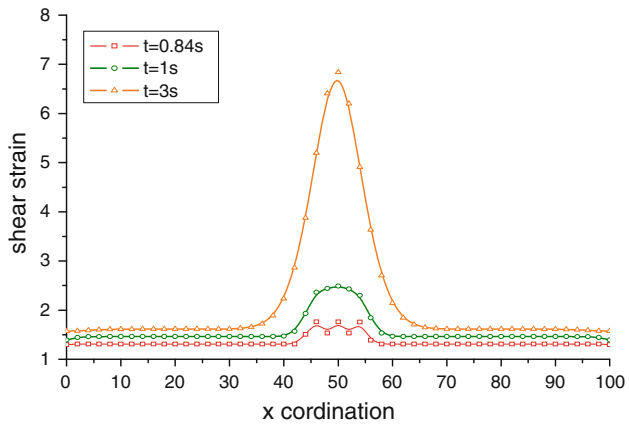

Fig. 12 The localization process of two FADs with four disturbances

until a nominal shear strain of 2.0 was reached. Thus, FADs with a certain amount of disturbance energy were very important for the occurrence of severe localization in a limited loading time. As far as shear banding is concerned, there seemed to be two distinct phases, separated by the localization strain γ_l. In the first stage ($\gamma < \gamma_l$), the finite amplitude disturbances coalesce, and the stress evolved close to that of a uniform solution. Then, in the second stage ($\gamma > \gamma_l$), localization occurred; the shear band shrank to its final form, the stress dropped drastically and the strain rate at the center of shear band increased sharply. In the localization stage a single shear band formed. This is qualitatively consistent with the experimental observations.

Furthermore, the effects of different aspects of finite amplitude disturbances on the evolution of shear bands were examined numerically. Firstly, the FADs imposed in the vicinity of γ_c lead to the lowest value of localization strain γ_l. The disturbances with the highest energy and shortest wavelength also led to the lowest value of localization strain. Secondly, the position of the final developed shear band depends on the distribution of FADs and not on any individual FAD. Finally, the distribution of FADs was found to have an important influence on the value of γ_l. Generally speaking, the easier the FADs coalesce the smaller the γ_l, i.e. the earlier the localization occurred.

As the material parameters adopted in the analysis were obtained by using the in situ soils in Beichuan, the evolution of shear banding characterizes the behavior of the soil layer, and the critical conditions for shear band formation can be used in the forecasting of landslides or debris flows in this area.

Acknowledgments This paper is supported by National Basic Research Program of China "Activity characteristics and formation rules of secondary mountain hazard of earthquake" (No. 2008CB425802) and Key Program of Chinese Academy of Sciences (No. KZCX2-YW-302-02).

References

Aifanti EC (1987) The physics of plastic deformation. Int J Plast 3:211–248

Bai YL (1982) Thermo-plastic instability in simple shear. J Mech Phys Solids 30(4):195–206

Bauer E, Huang WX, Wu W (2004) Investigations of shear banding in an anisotropic hypoplastic material. Int J Solids Struct 41(21):5903–5919

Cheng XQ, Li ZG, Cui P et al (2009) Estimation of soil erosion caused by the 5.12 Wenchuan Earthquake. J Mt Sci 27(1):122–127 (in Chinese)

Cui P (1992) Study on condition and mechanisms of debris flow initiation by means of experiment. Chin Sci Bull 37(9):759–763 (in Chinese)

Cui P, Wei FQ, He SM et al (2008) Mountain disasters induced by the earthquake of May 12 in Wenchuan and the disasters mitigation. J Mt Sci 26(3):280–282 (in Chinese)

Lade PV (1994) Instability and liquefaction of granular material. Comput Geotech 16(2):123–151

Lade PV, Nelson RB, Ito YM (1988) Instability of granular materials with non-associated flow. J Eng Mech ASCE 114:2173–2191

Loret B, Provest JH (1991) Dynamic strain localization in fluid-saturated porous media. J Eng Mech ASCE 117:907–922

lshibli KA, Sture S (2000) Shear band formation in plane strain experiments of sand. J Geotech Geoenviron Eng ASCE 126(6):495–503

Lu X (2001) On the shear instability of saturated soil. Int J Eng Sci 39:963–972

Lu XB, Cui P (2003) On the development of shear band by considering the strain gradient. Iran J Sci Technol 27(B1):57–62

Lu X, Zhang J, Yang Z (2000) On the evolution of shear bands in saturated soil. Int J Nonlinear Mech 35:21–26

Lu X, Wang S, Cui P (2004) An approximate method for shear bandwidth of shear band in saturated sands. Int J Numer Anal Methods Geomech 28:1533–1541

Oda M, Kazama H (1998) Microstructure of shear bands and its relation to the mechanisms of dilatancy and failure of dense granular soils. Geotechnique 48(4):465–481

Ottosen NS, Runesson K (1991) Properties of bifurcation solutions in elasto-plasticity. Int J Solids Struct 27:401–421

Peric D, Runesson K, Sture S (1992) Evaluation of plastic bifurcation for plane strain versus axisymmetry. J Eng Mech ASCE 118(3):512–524

Pietruszczak S (1995) Undrained responses of granular soil involving localized deformation. J Eng Mech ASCE 121(12):1292–1297

Rice JR (1975) On the stability of dilatant hardening for saturated rock masses. J Geophys Res 80(11):1531–1536

Rice JR, Cleary MP (1976) Some basic stress diffusion solutions for fluid-saturated elastic porous media with compressible contents. Rev Geophys Space Phys 14:227–241

Runesson K, Ottosen NS, Peric D (1991) Discontinuous bifurcations of elastic–plastic solutions at plane stress and plane strain. Int J Plast 7:99–121

Runesson K, Peric D, Sture S (1996) Effect of pore–fluid compressibility on localization in elastic–plastic porous solids under undrained conditions. Int J Solids Struct 33(10):1501–1518

Runesson K, Larsson R, Sture S (1998) Localization in hyperelasto-plastic porous solids subjected to undrained conditions. Int J Solids Struct 35:4239–4255

Tejchman J, Wu W (1996) Numerical simulation of shear band formation with a hypoplastic constitutive model. Comput Geotech 18(1):71–84

Vardoulakis I (1985) Stability and bifurcation of undrained, plane rectilinear deformations on water-saturated granular soils. Int J Numer Anal Methods Geomech 9:399–414

Vardoulakis I (1986) Dynamic stability analysis of undrained simple shear on water-saturated soils. Int J Numer Anal Methods Geomech 10:177–190

Vardoulakis I (2002) Dynamic thermo-poro-mechanical analysis of catastrophic landslides. Geotechnique 52(3):157–171

Vardoulakis I, Graf B (1985) Calibration of constitutive models for granular materials using data from biaxial experiments. Geotechnique 35:299–317

Xing D, Bai YL, Cheng CM et al (1991) On post-instability processes in adiabatic shear in hot rolled steel. J Mech Phys Solids 39(8):1017–1027